AGU ADVANCING EARTH AND SPACE SCIENCE

Geophysical Research Letters

RESEARCH LETTER
10.1029/2020GL089462

On the Impact of a Streaming Oxygen Population on Collisionless Magnetic Reconnection

Håkon Midthun Kolstø[1], Michael Hesse[1,2], Cecilia Norgren[1], Paul Tenfjord[1], Susanne Flø Spinnangr[1], and Norah Kwagala[1]

[1]Space Plasma Physics Group, University of Bergen, Bergen, Norway, [2]NASA Ames Research Center, CA, USA

Key Points:
- Tailward motion of the X-point is generated even though the oxygen is demagnetized
- The oxygen couples to the magnetic flux through electrostatic coupling with the electrons
- The momentum of the streaming oxygen does not affect the reconnection rate

Correspondence to:
H. M. Kolstø,
hakon.kolsto@uib.no

Citation:
Kolstø, H. M., Hesse, M., Norgren, C., Tenfjord, P., Spinnangr, S. F., & Kwagala, N. (2020). On the impact of a streaming oxygen population on collisionless magnetic reconnection. *Geophysical Research Letters*, *47*, e2020GL089462. https://doi.org/10.1029/2020GL089462

Received 22 JUN 2020
Accepted 21 OCT 2020
Accepted article online 29 OCT 2020

Abstract Using 2.5-D Particle-In-Cell (PIC) simulations, we investigate how magnetotail reconnection is affected by a cold, streaming, oxygen plasma population, attributed to an ionospheric source, in the inflow region. As the tailward streaming oxygen reaches the current layer, a tailward motion of the reconnection site is induced. Due to the much longer cyclotron period of the oxygen ions, oxygen cannot couple as directly into the reconnection dynamics as protons. We find that the oxygen ions couple indirectly by means of impacting the electron dynamics. Therefore, a demagnetized species can, in fact, alter the dynamics of the reconnection site. We see further that the reconnection rate remains unchanged relative to a nonstreaming run. Our results may prove useful for understanding the development and dynamics of magnetospheric substorms and storms.

1. Introduction

Magnetic reconnection is one of the primary energy conversion and transport mechanisms in space plasmas. It converts stored electromagnetic energy to thermal and kinetic energy of the plasma particles and is the motor behind large-scale phenomena such as particle acceleration, momentum, and magnetic flux transport throughout the magnetosphere and beyond. In order for reconnection to take place, the frozen-in condition needs to be violated (Vasyliunas, 1975); that is, the bulk motion of the electrons should decouple from the transport of magnetic flux.

In the plasma sheet, abundant species such as protons and electrons may at certain times be accompanied by heavier species as, for example, O^+ (Baker et al., 1982; Chappell et al., 1987; Moore et al., 2001). The presence of oxygen ions whose origin is from the high-latitude ionosphere has been observed in the Earth's magnetotail (Frank et al., 2012; Grande et al., 2013; Mouikis et al., 2018; Moore et al., 2001; Wilken et al., 1995; Zong et al., 1998), and the ionospheric outflow rate is proportional to geomagnetic activity (Baker et al., 1982). Spacecraft observations by Cluster reveal that O^+ may be the dominating ion species during storm time conditions (Kistler et al., 2005; Wygant et al., 2005). The GEOTAIL spacecraft observed bursts of tailward streaming oxygen ions of ionospheric origin in the magnetotail with a peak of the velocity distribution function (VDF) at 1,700 km/s (Wilken et al., 1995).

In this paper we investigate how the reconnection process is affected by a streaming oxygen population. Previous studies have shown that tailward streaming protons lead to a tailward motion of the X-point (Tenfjord et al., 2020). While the temperature of the inflow population does not seem to play a major role for the reconnection rate (Dargent et al., 2020; Divin et al., 2016; Tenfjord et al., 2019), its mass density does (Kolstø et al., 2020; Tenfjord et al., 2019). The inclusion of additional ion species has been shown to result in distinct spatial and time scales for the reconnection process (Divin et al., 2016; Shay & Swisdak, 2004; Toledo-Redondo et al., 2015). Compared to protons, the oxygen ions have a much larger cyclotron period, and thus, their coupling to the magnetic flux is less evident. Throughout the times of investigation, the oxygen ions in this simulation remain demagnetized. We here report on the effect a demagnetized streaming oxygen species has on the reconnection process.

The outline of this paper is as follows: Section 2 gives an overview of the simulation setup employed for this investigation. Section 3 examines the motion of the X-point, the evolution of the reconnection process, and the associated distribution functions. Finally, in section 4, we investigate how the reconnection rate is affected.

2. Simulation Setup

The analysis is performed by employing a 2.5-D Particle-In-Cell (PIC) simulation, that is, two spatial components and three field and velocity components, designed to model the magnetotail conditions during a burst of ionospheric oxygen outflow. The coordinate system is as follows: x is the reconnection outflow direction, y is the current direction, and z is the inflow direction. Initially, the magnetic field configuration is given by a generalized Harris-type equilibrium defined as $B_x = B_0 \tanh(z/\lambda)$, where $\lambda = 2d_p$ is the half width of the initial current sheet and $d_p = c/\omega_{pi} (= c\sqrt{m_p/4\pi n_0 e^2})$ is the proton inertial length. Densities are normalized to the foreground density at the center of the initial current sheet n_0.

A uniform proton distribution with a density of $n_b = 0.2$ is added to the initial Harris sheet density configuration $n_p = n_0/\cosh^2(z/2d_p)$ resulting in a peak density of 1.2 in the current layer. The protons initially have no x-directed bulk velocity. Oxygen ions are distributed homogeneously above a specific field line, corresponding to a distance of $|z| > 3d_p$ from the current sheet. The O^+ has initially zero thermal velocity but an x-directed bulk velocity of $v_x^{O^+} = 0.5v_A$, where v_A is the proton Alfvén velocity. The electrons associated with the oxygen ions have the same initial bulk velocity, that is, $v_x^e = 0.5v_A$, whereas the electrons initially accompanying the protons are stationary. When referring to tailward streaming O^+ of ionospheric origin, this setup presumes that the oxygen ions has been preaccelerated to move in the x-direction.

The following mass ratios are employed: $m_p/m_e = 25$ for the protons/electrons and $m_{O^+}/m_p = 16$ for the oxygen/protons. A total of $\sim 10^{10}$ macroparticles is used. Boundary conditions are periodic at $x = x_{min}$ and $x = x_{max}$. At $z = z_{min}$ and $z = z_{max}$, specular reflection is enabled and the out-of-plane electric field E_y is set to zero, preserving magnetic flux in the simulation domain.

Lengths are normalized to d_p, whereas time is normalized to the inverse of the proton cyclotron frequency $\Omega_p^{-1} = m_p/eB$. The size of our simulation domain is $410d_p \times 50d_p$ with a grid size of $6{,}400 \times 1{,}600$. We employ a time step of $\omega_{pe}\delta t = 0.5$. The velocity normalization is the proton Alfvén speed, based on the foreground current sheet density n_0. The foreground temperatures fulfill $T_p + T_e = 0.5$, in units of $(m_p v_A^2)$, derived from pressure balance $n_0(T_p + T_e) = \frac{B_0^2}{2}$ with $n_0 = 1$ and $B_0 = 1$, and the ratio of proton-electron temperature is chosen to be $T_p/T_e = 5$. The ratio between the electron plasma frequency and gyrofrequency is $\omega_{pe}/\Omega_e = 2$.

3. Motion of the Reconnection Site

Figure 1a shows the time evolution of the x-location of the X-point. Initially, the X-point is located at $x = 205d_p$. At $\Omega_p t = 50$, the X-point shows an earthward displacement due to the formation of an island. It is not until the oxygen ions reach the reconnection site at $\Omega_p t \approx 120$ that the X-point starts to move in the positive x-direction. When the oxygen density at the reconnection site is of significance, the X-point moves at the center-of-mass velocity, given by

$$v_c = \frac{\sum_i M_i v_{ix}}{\sum_i M_i} = 0.45, \quad \text{where} \quad M_i = m_i \int n_i \mathrm{d}x\mathrm{d}z \tag{1}$$

where the summation index i sums over all three species in the simulation domain and M_i is the total mass of the respective species. The oxygen ions are the main contributor to v_c due to their much higher momentum as compared to the other species.

The motion of the X-point is associated with a gradient of the y-component of the electric field by virtue of Faraday's law. As the oxygen ions are the drivers of the X-point motion, we investigate how E_y is supported by O^+, through Ohm's law, given by

$$E_y = m_{O^+}\left(\frac{\partial}{\partial t} v_y^{O^+} + \vec{v}_{O^+} \cdot \nabla v_y^{O^+}\right) + v_x^{O^+} B_z - v_z^{O^+} B_x + \frac{1}{n_{O^+}} \nabla \cdot \mathbf{P}^{O^+} \cdot \hat{y}$$

In Figure 1b, we see a clear gradient of E_y in the vicinity of the X-point. The finite gradient $\partial E_y/\partial x > 0$ results in a local decrease of the magnetic field as $\partial B_z/\partial t < 0$, leading to a tailward shift of the X-point. Furthermore, we see that E_y is sustained by a variety of contributors of comparable size, such as the Lorentz term and the inertia and pressure terms. Hence, the oxygen ions are not $\vec{E} \times \vec{B}$ drifting and thus not frozen-in. In Figure 1c, to the right of the X-point, we see that the oxygen density enhancement moves close to the magnetic flux velocity, even though the O^+ does not exhibit a magnetized behavior. This apparent motion of the O^+ density enhancement is strongly influenced by the z-motion of the oxygen ions.

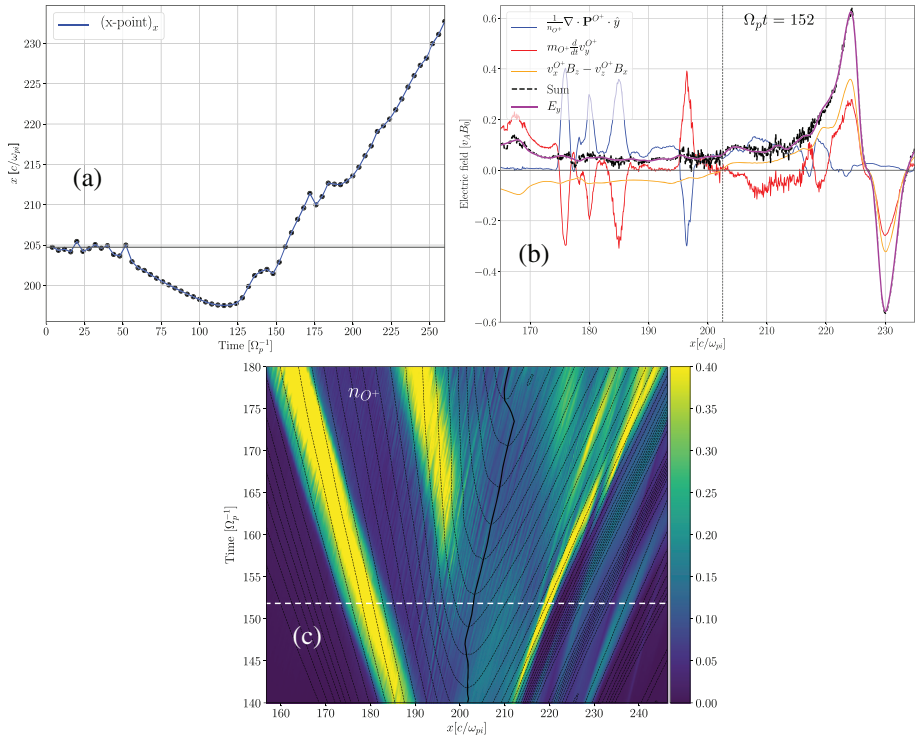

Figure 1. (a) Time of evolution of the x-location of the X-point showing its clear x-directed motion. (b) The y-component of Ohm's law for O^+. The vertical black dotted line is the location of the X-point. The black dotted line denotes the sum of the terms adding up to E_y. (c) A cut through the X-point along x following how the oxygen ion density evolves as a function of time. The color map shows n_{O^+}, the dotted line shows the contours of the magnetic vector potential A_y, defined by $\vec{B} = \nabla\vec{A} \times \hat{y} + B_y\hat{y}$, and the solid black line is the X-point location. This shows that the motion of the oxygen density enhancement moves close to the magnetic flux velocity. The white dotted horizontal line in (c) shows the time where the y-component of Ohm's law for O^+, in panel (b), is evaluated.

Since the velocity of the X-point is essentially determined by O^+, some mechanism must allow the oxygen ions to deliver their momentum to the magnetic flux tubes. As the electrons are well magnetized, we propose that there must be a coupling between O^+ and e^-. We speculate that this alignment may result from electrostatic coupling between O^+ and e^-, which enables an indirect coupling of the oxygen ions to the magnetic field. In the next section we explore how such a coupling occurs.

3.1. Electrostatic Coupling Between O^+ and e^-

Even though the oxygen ions are not $\vec{E} \times \vec{B}$ drifting, they move close to the magnetic flux velocity as seen in the local density enhancement to the right of the X-point in Figure 1c. In Figure 2a, we see the frozen-in behavior of the electrons, as $E_y \approx v_x^e B_z$ which implies that the magnetic flux is moving with the electrons as $v_z^e B_x \approx 0$. This is suggestive of some underlying mechanism, which enables the coupling between the oxygen ions and the electrons. We investigate this by evaluating the electron momentum equation, given by

$$m_e n_e \left(\frac{\partial}{\partial t}\vec{v}_e + \vec{v}_e \cdot \nabla\vec{v}_e \right) = -n_e(\vec{v}_e \times \vec{B} + \vec{E}) - \nabla \cdot \mathbf{P}^e$$

across the local density enhancement, indicated by the peak of n_e and n_{O^+} occurring at $x \approx 218 d_p$ and $\Omega_p t = 152$.

By studying the x-component, we can investigate how the actual coupling takes place. Leading up to the density enhancement seen in Figure 2b at $x \approx 218 d_p$, we see a sharp increase in the pressure gradient. The enhanced O^+ density binds the electrons, and this configuration is kept stable by the x-component of the electric field. The pressure gradient of the electrons is directed toward the density peak and attempts to diffuse this enhancement but are instead kept together by electric forces such that $\partial_x P_{xx}^e \approx -en_e E_x$ is fulfilled.

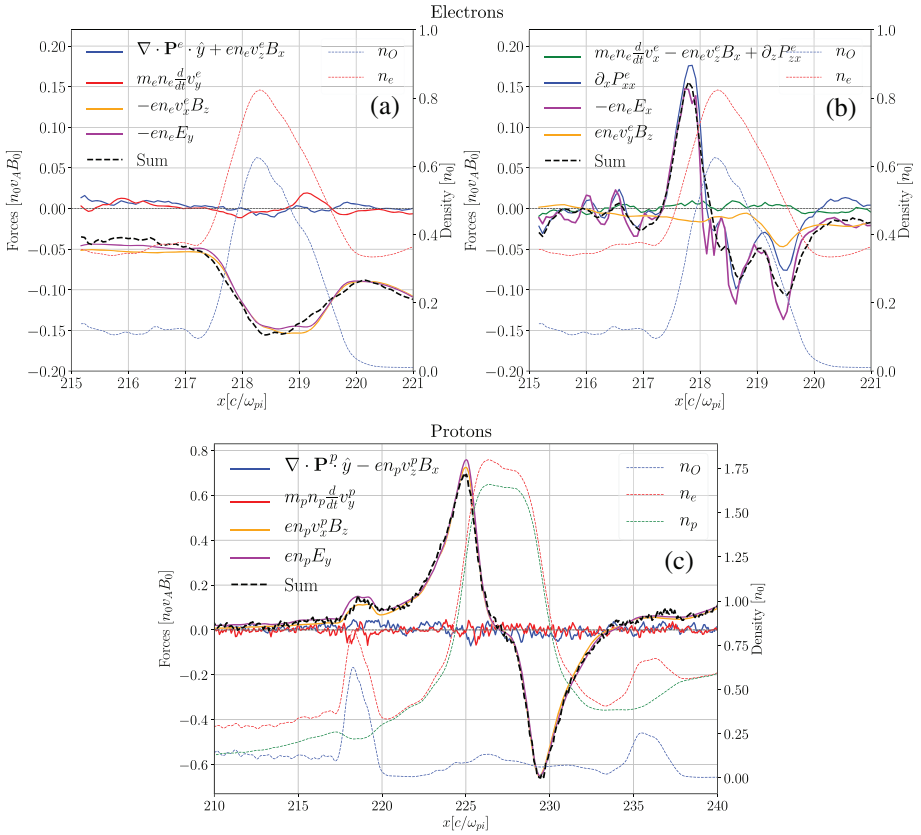

Figure 2. Cut through the X-point, along the x-direction, showing (a) the y-component and (b) the x-component of the momentum equation for electrons. Panel (c) shows the y-component of the momentum equation for the protons over a larger region in the x-direction, which reveals the frozen-in behavior of the protons. At $x \approx 218 d_p$, we see the clear n_O and n_e enhancements where the electrostatic coupling is most profound. From the low-density gradient of the protons in this region, we see that they do not, strongly, take part in the electrostatic coupling. The momentum equation for both the protons and electrons is calculated between $\Omega_p t = 152 - 152.5$. The black dotted line is the sum of the terms adding up to $-en_e E_y$.

This electrostatic coupling now forces the e^- to move with the O^+. In turn, this induced electron motion leads to the flux transport consistent with the X-point motion. Shown in Figure 2c, the protons also display frozen-in behavior as $E_y + v_x^p B_z \approx 0$. Hence, they are moving with the magnetic flux as well, at the cost of a small fraction of the oxygen ion's momentum.

3.2. Evaluation of Coupling With a Lower O^+ Density Run

In order to test if such a coupling still occurs with a substantially lower O^+ density, we perform a simulation with the same conditions as described in section 2, except with an oxygen number density of a tenth of the first shown run, that is, $n_{O^+} = 0.02$. In this case, we also observe an x-directed motion of the X-point moving at approximately the center-of-mass velocity, which now is $v_c = 0.25$. The electrostatic coupling between O^+ and e^- is less profound but remains adequate to result in a clear motion of the X-point. In Figures 3a and 3b we see the clear motion of the X-point together with the matching motion of the oxygen ions and the magnetic flux seen to the right of the X-point. When the oxygen content in the reconnection region is of significance, and the X-point starts moving at approximately v_c, we evaluate the electron momentum equation over the rightmost n_{O^+} enhancement at $\Omega_p t = 184$, indicated by the white line in Figure 3b. In Figure 3c, we see the frozen-in behavior of the electrons over the density enhancements as $E_y \approx v_x^e B_z$. Furthermore, Figure 3d reveals the same manifestation as the high oxygen density, seen in Figure 2b, run with the pressure gradient $\partial_x P_{xx}^e$ balanced by the electric force $-en_e E_x$, thus permitting a coupling between O^+ and e^-. From this, we conclude that such a coupling may still occur even with a substantial reduction of the oxygen abundance.

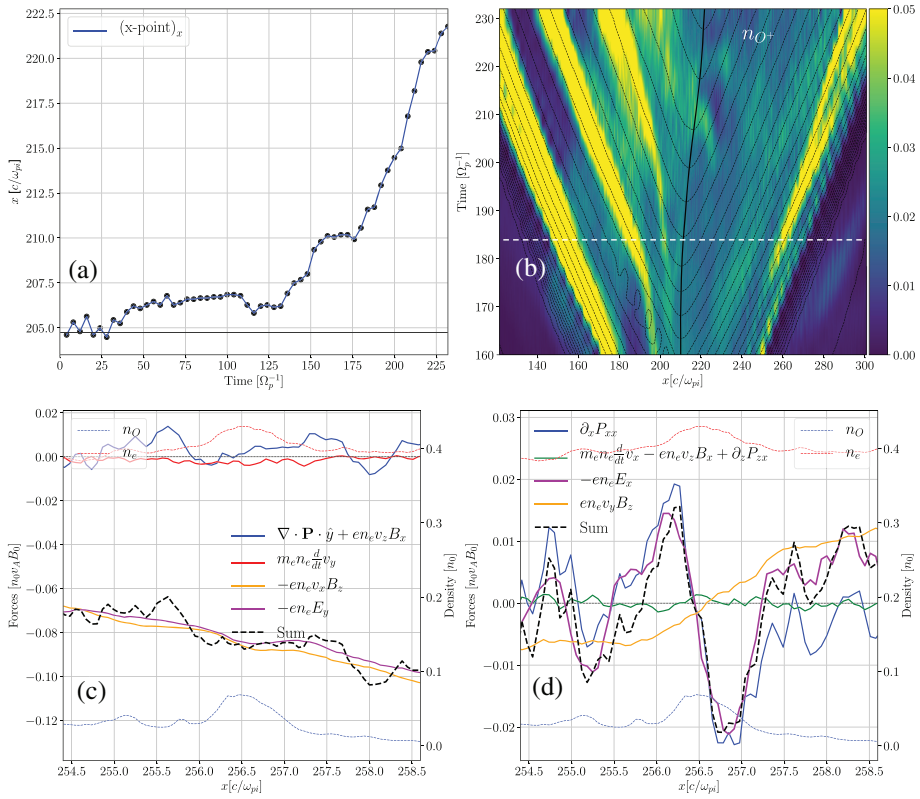

Figure 3. Panels (a) and (b) display the X-point motion as well as the n_{O^+} evolution (same as seen in Figure 1) for the low-density run. The white dotted line in (b) shows the region of calculation of the y-component and x-component of the electron momentum equation in (c) and (d), respectively. The electron momentum equation is calculated at $\Omega_p t = 184$.

3.3. Density Striations

In this section we investigate the intricate density striations, seen in Figures 4a–4c, which, as we will see, can be attributed to the additional x-directed momentum of O^+. In Figure 4a, we see the formation of an oxygen wave, due to the collective acceleration of O^+ by the Hall electric field E_z, thus leaving behind a density cavity (Tenfjord et al., 2018). This is the same manifestation as for the nonstreaming case, but as the system evolves, new types of striations arise as a result of the oxygen's more complicated interactions with E_z prior to reaching the reconnection site. This interaction results in more complex distribution functions specific to the streaming case, and an example is shown in Figures 4d–4f. The VDF is extracted at the oxygen wave front shown in Figures 4a–4c at time $\Omega_p t = 140$. It reveals, as shown in Figures 4d–4f, three dominant populations with clear separation in v_z. In order to understand the origin of the density striations, we follow two oxygen test particles from Populations (1) and (2), shown in Figure 4. Their initial conditions are selected as the most probable phase-space coordinate for the respective population. As the system is symmetric in z, Population (3) exhibits the same features as Population (1), only with the opposite z-direction of the velocity.

Figures 4g and 4h show the trajectories of the test particles from Populations (1) and (2) which have been traced $\pm 20\Omega_p^{-1}$ in dynamically changing fields with a time step of $0.5\Omega_p^{-1}$ from $\Omega_p t = 140$ by the initial conditions obtained from the VDF shown in Figures 4d–4f. Dependent on the regions at which O^+ originates from, they interact differently with the Hall electric field E_z. This can be seen in Figures 4i and 4j, which show the forces acting on the test particles from the respective populations.

The test particle from Population (1), seen in Figures 4g and 4h as the white trajectory, originates from further out in the lobe and experiences a much stronger acceleration as it encounters a different E_z region. Seen in Figure 4i, its substantially higher v_z enables it to overcome the electric potential and continue its motion out to the lobes before it is reflected by the Lorentz force due to $-v_z B_x$ and subsequently $v_y B_x$. Particles that exhibit similar properties trace out the outermost striations evident in Figure 4c. The test particle from

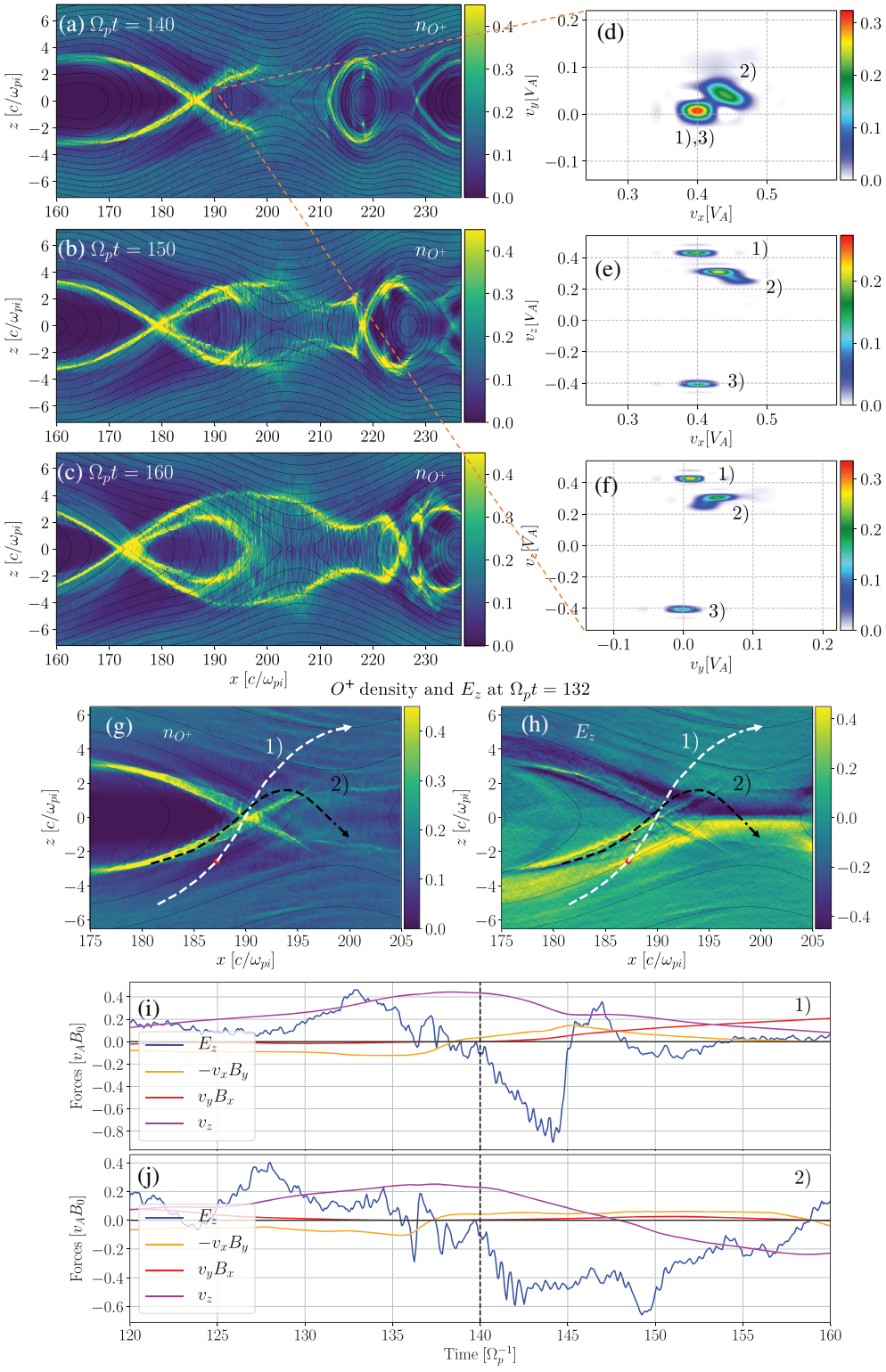

Figure 4. (a–c) Time of evolution of the oxygen density for the high n_{O^+} run. (d–f) VDF extracted at $(\Omega_p t, x, z) = (140, 190.5d_p, 0.5d_p)$. (g, h) Particle tracing of Populations (1) (white) and (2) (black) where the color map shows the (a) O^+ density and (b) E_z at $\Omega_p t = 132$. The red dots shows the location of the O^+ test particles at $\Omega_p t = 132$. Panels (i) and (j) show the forces in the z-direction acting on particles from Populations (1) and (2), respectively. The vertical dotted line in black shows the initial time of tracing.

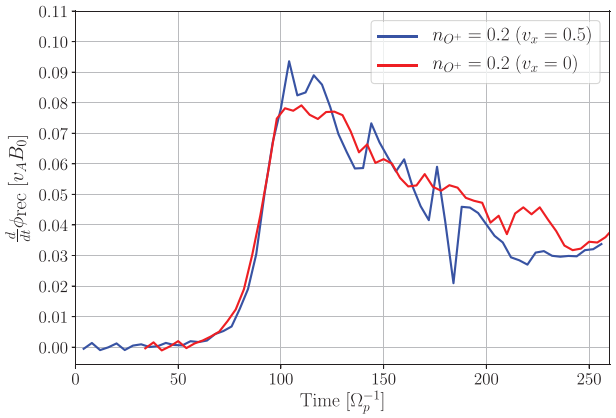

Figure 5. Time of evolution of the reconnection rate expressed as the temporal change of the magnetic flux $\frac{d}{dt}\phi_{\mathrm{rec}}$. In blue: streaming run. Red: nonstreaming run.

Population (2), seen in Figures 4g and 4h as the black trajectory, travels along the clear density enhancement upon interacting with E_z. The E_z this particle encounters is not strong enough for it to be accelerated to a sufficiently high v_z to overcome the electric potential on the opposite side of the current sheet; see Figure 4j. It is thus reflected in the z-direction by E_z and proceeds with a bounce motion across the current sheet until it reaches the exhaust. Such particles trace out the innermost striation seen in Figure 4c.

Particles originating from Populations (1) and (3) both trace out the outer striations as they share similar acceleration histories, only from the southern and northern lobes, respectively. These particles are collectively accelerated by the Hall electric field, which forms an oxygen wave leaving behind a density cavity (Tenfjord et al., 2018). As the Hall electric field expands, oxygen ions further into the lobes are accelerated toward the diffusion region causing an expansion in the z-direction of the outermost striations. Figures 4a–4c and 1b create the impression of an outflow of oxygen ions toward the Earth—counter to the original tailward motion of the O^+. This apparent motion in the negative x-direction is solely the result of an earthward shift of the intersection between the outer striations as they expand. There are therefore not indications of any transport of O^+ in the negative x-direction.

The striations discussed in this section may be observed by spacecraft, but it is, in principle, possible that they are unstable to various waves. In the simulation, the velocity of the O^+ is small compared to the thermal velocity of the protons and the electrons, and thus, it is less likely that the oxygen ions will drive any instabilities. However, other instabilities could, of course, cause fluctuations in the Hall electric field that accelerates O^+ and therefore impact the integrity of the structures.

4. Reconnection Rate

The evolution of the reconnection rate is displayed in Figure 5. We compare the reconnection rate to a similar run with the same oxygen number density n_{O^+} but with no initial x-directed bulk velocity, hereafter referred to as the nonstreaming run. Compared to the nonstreaming run, the reconnection process reaches its fast phase at a later time due to a smaller initial perturbation. For illustrations purposes, we shift the nonstreaming run by $\Omega_p t = 30$ to have the fast phases aligned.

We do notice a slightly higher peak for the streaming run. This is a transient effect as a result of the low abundance of oxygen ions at the reconnection site. The difference between the distance of the initial location of the front of the oxygen ions to the current sheet is slightly larger for the streaming run. This allows, to a greater extent compared to the nonstreaming run, an unencumbered motion of the upstream magnetic flux tubes, which results in a faster reconnection rate. The reconnection process therefore proceeds faster until the density of the oxygen ions in the reconnection site becomes significant. From this we conclude that a streaming population does not impose any further reduction of the reconnection rate.

5. Discussion and Summary

Motivated by ionospheric outflow, the results provided in this paper provide insights into how a streaming demagnetized species alter the dynamics of the reconnection process. We have shown that the X-point moves with the center-of-mass velocity v_c, which is predominantly provided by the oxygen ions.

Tenfjord et al. (2020) performed a similar study with the protons as the streaming population and found that the X-point also moves with v_c. The protons remain magnetized in the exhaust, and thus, their coupling to the magnetic field is evident. Having oxygen ions as the streaming population, however, is considerably different as they do not exhibit a magnetized behavior throughout the times of investigation. Our findings show that a demagnetized species alters the dynamics of the reconnection site long before the time of magnetization is realized. The coupling of O^+ to the magnetic flux occurs instead indirectly through the electrons by an electrostatic coupling. This shows that, regardless of whether the streaming population is magnetized or

not, the system will reorganize itself in such a manner as to retain a net zero outflow momenta in the frame of reference of the X-point.

Compared to a nonstreaming run (e.g., Tenfjord et al., 2018), a streaming population gives rise to involved distribution functions due to the interaction with the Hall electric field E_z. The O^+ populations shown in Figures 4d–4f trace out the distinct striations seen in Figure 4c. Regarding observations, the VDF shown here should be detectable by spacecraft, but may be modified by kinetic effects not included in our simulation. Furthermore, our results show that a streaming population does not impose any change to the reconnection rate.

The results obtained in this study may apply to magnetotail reconnection in case of ionospheric outflow which results in high momentum O^+. With regard to space applications, we hope that the results laid out in this paper provide useful insight for future analysis of space mission data, in particular, the Magnetospheric Multiscale mission.

Data Availability Statement

Data set used in this analysis is available at Kolstø (2020).

Acknowledgments
This study was supported by the University of Bergen, by NOTUR/NORSTOR under project NN9496K, and by NASA's MMS mission. P. Tenfjord and C. Norgren was supported by the Research Council of Norway under contract 300865.

References

Baker, D. N., Hones, E. W., Young, D. T., & Birn, J. (1982). The possible role of ionospheric oxygen in the initiation and development of plasma sheet instabilities. *Geophysical Research Letters*, *9*(12), 1337–1340. https://doi.org/10.1029/GL009i012p01337

Chappell, C. R., Moore, T. E., & Waite, J. H. (1987). The ionosphere as a fully adequate source of plasma for the Earth's magnetosphere. *Journal of Geophysical Research*, *92*(A6), 5896–5910. https://doi.org/10.1029/JA092iA06p05896

Dargent, J., Aunai, N., Lavraud, B., Toledo-Redondo, S., & Califano, F. (2020). Simulation of plasmaspheric plume impact on dayside magnetic reconnection. *Geophysical Research Letters*, *47*, e2019GL086546. https://doi.org/10.1029/2019GL086546

Divin, A., Khotyaintsev, Y. V., Vaivads, A., André, M., Toledo-Redondo, S., Markidis, S., & Lapenta, G. (2016). Three-scale structure of diffusion region in the presence of cold ions. *Journal of Geophysical Research: Space Physics*, *121*, 12,001–12,013. https://doi.org/10.1002/2016JA023606

Frank, L. A., Ackerson, K. L., & Yeager, D. M. (2012). Observations of atomic oxygen (O+) in the Earth's magnetotail. *Journal of Geophysical Research*, *82*(1), 129–134. https://doi.org/10.1029/JA082i001p00129

Grande, M., Perry, C. H., Hall, A., Fennell, J., Nakamura, R., & Kamide, Y. (2013). What is the effect of substorms on the ring current ion population during a geomagnetic storm? *American Geophysical Union (AGU)*, *142*, 75–89. https://doi.org/10.1029/142GM08

Kistler, L. M., Mouikis, C., Möbius, E., Klecker, B., Sauvaud, J. A., Réme, H., et al. (2005). Contribution of nonadiabatic ions to the cross-tail current in an O+ dominated thin current sheet. *Journal of Geophysical Research*, *110*, A06213. https://doi.org/10.1029/2004JA010653

Kolstø, H. M. (2020). Replication data for: On the impact of a streaming oxygen population on collisionless magnetic reconnection. DataverseNO, https://doi.org/10.18710/AG7QVS

Kolstø, H. M, Hesse, M., Norgren, C., Tenfjord, P., Spinnangr, S. F., & Kwagala, N. (2020). Collisionless magnetic reconnection in an asymmetric oxygen density configuration. *Geophysical Research Letters*, *47*, e2019GL085359. https://doi.org/10.1029/2019GL085359

Moore, T. E., Chandler, M. O., Fok, M.-C., Giles, B. L., Delcourt, D. C., Horwitz, J. L., & Pollock, C. J. (2001). Ring currents and internal plasma sources. *Space Science Reviews*, *95*(1-2), 555–568. https://doi.org/10.1023/A:1005264907107

Mouikis, C. G., Kistler, L. M., Liu, Y. H., Klecker, B., Korth, A., & Dandouras, I. (2018). H+ and O+ content of the plasma sheet at 15-19 Re as a function of geomagnetic and solar activity. *Journal of Geophysical Research: Space Physics*, *115*, A00J16. https://doi.org/10.1029/2010JA015978

Shay, M. A., & Swisdak, M. (2004). Three-species collisionless reconnection: Effect of O^+ on magnetotail reconnection. *Physical Review Letters*, *93*(17), 175001. https://doi.org/10.1103/PhysRevLett.93.175001

Tenfjord, P., Hesse, M., & Norgren, C. (2018). The formation of an oxygen wave by magnetic reconnection. *Journal of Geophysical Research: Space Physics*, *123*, 9370–9380. https://doi.org/10.1029/2018JA026026

Tenfjord, P., Hesse, M., Norgren, C., Spinnangr, S. F., & Kolstø, H. (2019). The impact of oxygen on the reconnection rate. *Geophysical Research Letters*, *46*, 6195–6203. https://doi.org/10.1029/2019GL082175

Tenfjord, P., Hesse, M., Norgren, C., Spinnangr, S. F., Kolstø, H., & Kwagala, N. (2020). Interaction of cold streaming protons with the reconnection process. *Journal of Geophysical Research: Space Physics*, *125*, e2019JA027619. https://doi.org/10.1029/2019JA027619

Toledo-Redondo, S., Vaivads, A., André, M., & Khotyaintsev, Y. V. (2015). Modification of the Hall physics in magnetic reconnection due to cold ions at the Earth's magnetopause. *Geophysical Research Letters*, *42*, 6146–6154. https://doi.org/10.1002/2015GL065129

Vasyliunas, V. M. (1975). Theoretical models of magnetic field line merging. *Reviews of Geophysics*, *13*(1), 303–336. https://doi.org/10.1029/RG013i001p00303

Wilken, B., Zong, Q. G., Daglis, I. A., Doke, T., Livi, S., Maezawa, K., et al. (1995). Tailward flowing energetic oxygen ion bursts associated with multiple flux ropes in the distant magnetotail: GEOTAil observations. *Geophysical Research Letters*, *22*(23), 3267–3270. https://doi.org/10.1029/95GL02980

Wygant, J. R., Cattell, C. A., Lysak, R., Song, Y., Dombeck, J., McFadden, J., et al. (2005). Cluster observations of an intense normal component of the electric field at a thin reconnecting current sheet in the tail and its role in the shock-like acceleration of the ion fluid into the separatrix region. *Journal of Geophysical Research*, *110*, A09206. https://doi.org/10.1029/2004JA010708

Zong, Q.-G., Wilken, B., Woch, J., Mukai, T., Yamamoto, T., Reeves, G. D., et al. (1998). Energetic oxygen ion bursts in the distant magnetotail as a product of intense substorms: Three case studies. *Journal of Geophysical Research*, *103*(A9), 20,339–20,363. https://doi.org/10.1029/97JA01146